The stability of Co_3O_4, Fe_2O_3, Au/Co_3O_4 and Au/Fe_2O_3 catalysts in the catalytic combustion of lean methane mixtures in the presence of water

Adi Setiawan [a,b], Eric M. Kennedy [a], Bogdan Z. Dlugogorski [c],
Adesoji A. Adesina [d], Michael Stockenhuber [a,*]

[a] Priority Research Centre for Energy (PRCfE), Discipline of Chemical Engineering, School of Engineering, The University of Newcastle, Callaghan, NSW 2308, Australia
[b] Jurusan Teknik Mesin, Fakultas Teknik, Universitas Malikussaleh, Reuleut, Aceh Utara 24355, Indonesia
[c] School of Engineering and Information Technology, Murdoch University, Murdoch, WA 6150, Australia
[d] ATODATECH LLC, Brentwood, CA 94513, USA

ARTICLE INFO

ABSTRACT

Nano-sized Co_3O_4, Fe_2O_3, Au/Co_3O_4 and Au/Fe_2O_3 catalysts were prepared and evaluated for catalytic combustion of lean methane-air mixtures. Characteristics and catalytic activities under dry and wet feed conditions were investigated at gas hourly space velocities up to $100\,000\,h^{-1}$ mimicking the typical flow and conversion requirements of a catalytic system designed to treat a ventilation air methane stream. In order to gain a better understanding of the interaction between H_2O and the catalyst surface, temperature-programmed desorption of water over fresh and used samples were studied, and supported by other catalyst characterization techniques such as N_2-adsorption desorption, XRD, TEM, SEM and XPS analyses. The activity measurements of the catalysts studied identify Co_3O_4 as the most active material. Co-precipitating gold particles with cobalt oxide or iron oxide do not enhance the activity of the catalyst, which is most likely due to blocking the active site of support by the gold particle. The presence of strong hydroxyl bonds on the catalyst surface is substantiated by TPD and XPS analyses, and is suggested to be responsible for the rapid deactivation of Fe_2O_3 and Au/Fe_2O_3 catalysts.

© 2014 Elsevier B.V. All rights reserved.

1. Introduction

The anthropogenic emission of methane is emerging as an important environmental issue due to the volumes of the gas being emitted and the significant impact this has on the environment. Approximately 70% of methane emissions can be attributed to ventilation air methane (VAM) emitted from coal mines [1,2]. The large volumetric flow rate and the low methane concentration ($\leq 1\%$) of VAM stream presents a major challenge in developing technologies to mitigation or utilize this emission. A number of processes have been developed to mitigate these emissions. One potential solution for reducing methane emission is catalytic combustion, where methane is oxidized to carbon dioxide on a catalytically-active solid surface. This flameless combustion is ideal for highly diluted air/methane streams, as the production of NO_x is essentially absent and the reaction temperature is relatively low.

The catalytic combustion of methane has been extensively investigated over noble metals, transition metal oxides and mixed metal oxides. Pd-based catalysts are considered as one of the most active [3], however susceptibility to poisoning by water is a major practical problem when the catalyst is employed in a VAM stream as the humidity level of the stream is at or near saturation. As reported in our previous work, the water vapour present in the feed is the primary factor leading to catalyst deactivation observed during catalytic combustion of simulated VAM stream over 1100 h [4]. Therefore, the application in the VAM combustion necessitates the development of durable catalysts, characterized by improved resistance to water vapour-poisoning.

Gold was initially believed to be inactive as a catalyst because of its inability to chemisorb most gases under typical reaction conditions [5]. However, in a seminal study pioneered by Haruta et al., it was shown that carbon monoxide could be oxidized over gold catalysts [6] at temperatures as low as 77 K. This success

---

was followed by the development of a gold catalyst for the total methane oxidation [7], in which nano-sized gold catalysts were supported on various metal oxides [8,9] with the aim of improving the activity and stability of catalysts. The activity of supported gold catalysts during total oxidation of methane was reported recently [10,11], and although supported gold catalysts are not as active as palladium-based catalysts, an understanding on the nature of nano-sized gold can further our understanding of the deactivation process and in turn how to enhance the catalyst activity and stability. Limited measurements exist regarding the characteristics and catalytic activity of supported gold catalyst specifically for combustion of lean methane–air mixtures. Methane combustion in the presence of water over gold-based catalysts has not yet been investigated in detail.

Transition metal oxides have been considered as catalysts for total oxidation of methane due to their higher stability and lower cost when compared to noble metals [12]. Earlier work reported the use of single-metal oxides (such as Cr_2O_3, NiO, Mn_2O_3, Co_3O_4, and CuO) and these studies evaluated the activities and deactivation phenomena during lean methane combustion [13]. Among those tested, Co_3O_4 was the most active catalyst but was less stable compared to Mn_2O_3. Preparing different morphologies of cobalt oxide was demonstrated recently as a strategy for improving the catalytic activity [14]. Enhanced activity and stability was reported for Co_3O_4 nanotubes prepared using a morphology-directed technique [15]. The higher activity observed from these nanotubes catalysts was reported to be due to the prominence and exposure of the (1 1 2) crystal plane and high reactivity of the surface oxygen. However, the issue of catalyst stability in the presence of water vapour in the feed has not been addressed yet.

This paper reports the effect of water vapour present in catalytic combustion of lean methane mixture over pure oxide (Co_3O_4 and Fe_2O_3) and supported gold (Au/Fe_2O_3, Au/Co_3O_4) catalysts. The catalyst characteristics and catalytic activities under dry and wet feed are investigated at gas hourly space velocities (GHSVs) up to $100\,000\,h^{-1}$, mimicking the requisite conditions of a catalytic reactor used in large scale treatment of ventilation air methane stream. An understanding of the inhibitory effect of water vapour is explored by performing the temperature-programmed desorption of water from fresh and used samples supported by other characterization techniques such as N_2 adsorption desorption, XRD, TEM, SEM and XPS analyses.

2. Experimental

2.1. Catalyst preparation

Cobalt oxide was prepared using a precipitation method. $Co(NO_3)_2 \cdot 6H_2O$ (Sigma–Aldrich) was dissolved in water (0.1 M), the solution was stirred at $80\,°C$ and cobalt species precipitated by adjusting to a pH of 9 using Na_2CO_3 solution (0.25 M). The resulting precipitate was filtered, washed with hot and cold water and dried in an oven at $110\,°C$ for 20 h. Prior to catalyst activity measurement, the sample was pre-treated ex situ in air at $400\,°C$ for 4 h.

In order to investigate the effect of surface area on the catalytic activity and stability of iron oxide, a high surface area Fe_2O_3 catalyst was prepared by adding 0.33 mL of an aqueous solution of 0.36 M $Al(H_2PO_4)_3$ (Alfa Aesar) into 15.1 mL of 2.33 M $Fe(NO_3)_3$ (Sigma–Aldrich) [16]. The mixture was then placed in a rotary evaporator at $60\,°C$ for 2 h before being heated in a furnace to $380\,°C$ at a ramp of $4\,°C\,min^{-1}$ for 1 h. The resulting paste was then dried in an oven at $110\,°C$ for approximately 20 h, and calcined in static air at $400\,°C$ for 4 h to activate the catalyst as well as remove any residual phosphorus and nitrate originating from sample precursors. Finally the sample was purged with helium for 30 min prior to reaction.

Supported gold catalysts were prepared using a co-precipitation method [10]. For Au/Fe_2O_3 catalyst, a solution of 35.1 g of $Fe(NO_3)_3 \cdot 9H_2O$ (Sigma–Aldrich) was dissolved to form a solution of approximately 0.1 M. This solution was mixed with 0.3 g of $HAuCl_4 \cdot 3H_2O$ (Acros-Organic) dissolved in HCl (0.58 M). The solution was adjusted to a pH of 9 while being stirred at $80\,°C$ using Na_2CO_3 solution (0.1 M). The resulting precipitate was filtered under vacuum and washed with hot and then cold water several times. The precipitate was collected and dried in an oven at $110\,°C$ for approximately 16 h and pressed and sieved to 250–425 μm. The sample was then pre-treated ex situ in air at $400\,°C$ for 4 h, activating the catalyst as well as ensuring the removal of any residual precursors.

A similar method was used for preparing 2.2 wt.% Au/Co_3O_4 catalyst where 23.97 g of $Co(NO_3)_2 \cdot 6H_2O$ (Sigma–Aldrich) dissolved in water (0.1 M) was mixed with 307.2 mg of $HAuCl_4 \cdot 9H_2O$ (Acros-Organic) dissolved in HCl at $0.58\,mol\,L^{-1}$. The solutions were stirred at $80\,°C$ and Na_2CO_3 solution (0.25 M) was added drop wise until a pH of 8.2 was reached [10]. The resulting paste was then filtered, washed, dried and calcined under the same procedure as described above.

2.2. Catalytic activity measurement

Catalytic activity measurements were performed in a tubular stainless steel micro reactor. The inlet methane concentration was set at 0.6%, balanced with air at GHSVs between 27 000 and $200\,000\,h^{-1}$. The inlet and outlet mixtures were analyzed using a gas chromatograph equipped with a thermal conductivity detector (TCD) and concentric packed column (Alltech CTR-I). For humid feed experiments, the reactant mixture was passed through a saturator operated at $25\,°C \pm 3\,°C$ with a humidity probe installed at the outlet. The actual reaction temperatures were measured by placing a K-type thermocouple into the reactor close to the catalyst bed.

2.3. Catalyst characterization

The surface areas of catalysts were measured by nitrogen adsorption at 77 K using Gemini 11 2370 surface area analyser according to the Brunauer–Emmet–Teller (BET) method. Powder X-ray diffraction (XRD) patterns of catalysts were examined using Cu Kα radiation performed by a Philips X'Pert diffractometer in the range of 2θ angles from $2°$ to $90°$ with $0.008°$ 2θ step resolution. Temperature-programmed desorption (TPD) analyses were performed using a purpose built TPD apparatus equipped with Pfeiffer Prisma quadrupole mass analyser. Zeiss Sigma VP FESEM served to capture the scanning electron microscopy (SEM) images of the sample using a secondary electron (SE) detector and back-scattered electron (BE) detector. Bruker light element SSD Energy-dispersive X-ray spectroscopy (EDS) detector allowed the elemental analysis while capturing the SEM images. A JEOL 2100 Transmission Electron Microscope (TEM) was used for TEM imaging of supported gold catalysts. The gold loadings were quantified using Varian 715-ES inductively coupled plasma optical emission spectrometer (ICP-OES).

For surface analysis, ex situ X-ray photoelectron spectroscopy (XPS) was carried out using mono-chromated Al K alpha (energy 1486.68 eV) radiation and the emitted photoelectrons were analyzed using an ESCALAB250Xi manufactured by Thermo Scientific, UK. The energy scale was shifted relative to the adventitious carbon at 284.6 eV and the spectrometer was calibrated against binding energies of Au $4f_{7/2} = 83.96$ eV, Ag $3d_{5/2} = 368.21$ eV and Cu $2p_{3/2} = 932.62$ eV.
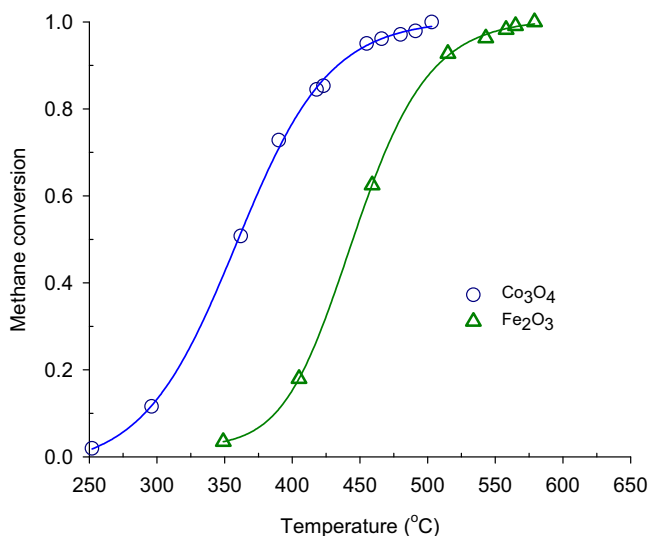
Fig. 1. Methane conversion as a function of temperature over (◯) Co_3O_4 and (△) Fe_2O_3 catalysts. Reaction condition: 6000 ppm CH_4 balance air at GHSV = 100 000 h^{-1}.

3. Results and discussions

3.1. The activity and stability of Co_3O_4 and Fe_2O_3 catalysts
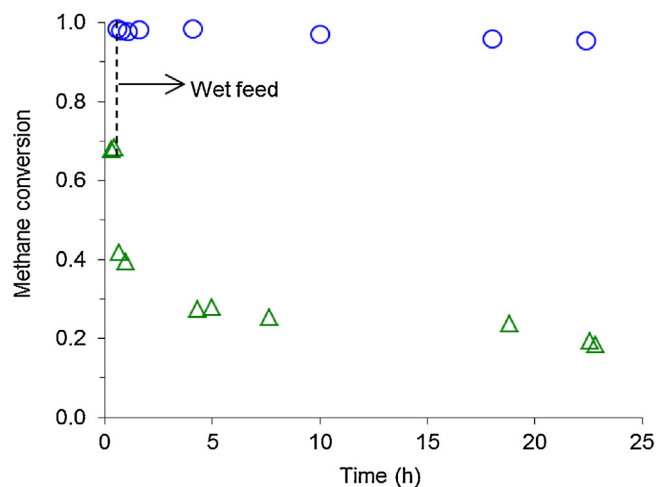
The catalytic activity tests of single oxide catalysts were performed by feeding the reactor tube with 6000 ppm methane (balance air) at gas hourly space velocity (GHSV) of 100 000 h^{-1}. The light-off curves were recorded at temperatures from 250 to 650 °C. A blank experiment was carried our prior to catalytic activity test and confirmed that no methane conversion was observed up to a temperature of 650 °C [17].

Fig. 1 shows the temperature dependency of methane conversion over Co_3O_4 and Fe_2O_3 catalysts. The temperature of 90% conversion varies significantly, with the Co_3O_4 exhibiting the lowest light-off temperature. The temperature at 90% methane conversion (T_{90}) for Co_3O_4 is 440 °C, while T_{90} of Fe_2O_3 is about 510 °C. These light-off curves clearly suggest that the nano-sized cobalt oxide is more active compared to Fe_2O_3 catalysts.

The stability of each catalyst was observed during time-on-stream (TOS) experiments under dry and humid feed conditions at reaction temperature of 455 °C and gas hourly space velocity of 100 000 h^{-1}. Initially, the methane combustion was carried out using a dry feed and after 1 h the reaction mixture was passed through a saturator and remained so continuously for 1 or 2 days. Fig. 2 shows the time-on-stream evolution of methane oxidation over Co_3O_4 and Fe_2O_3 catalysts. Adding water vapour into the feed produced no measurable drop in activity over the Co_3O_4 catalyst within 24 h TOS. Prolonging the operation up to 55 h under humid feed condition, the methane conversion level remained relatively constant, ranging from 95% to 98%. When compared to the Fe_2O_3 catalyst, a significant deactivation was observed where the methane conversion dropped from ca. 70% to 20% within 24 h under humid feed, suggesting that iron oxide activity is very sensitive to water compared to cobalt oxide.

3.2. The characteristic of Co_3O_4 and Fe_2O_3 catalysts

Nitrogen adsorption–desorption isotherms of Co_3O_4 and Fe_2O_3 catalysts are provided in Fig. S1 of supplementary information (SI), suggesting type IV isotherms from hysteresis loop observed within a relative pressure (p/p_0) range of 0.4–0.9 [18]. The surface area of the samples, calculated using the BET equation, results in
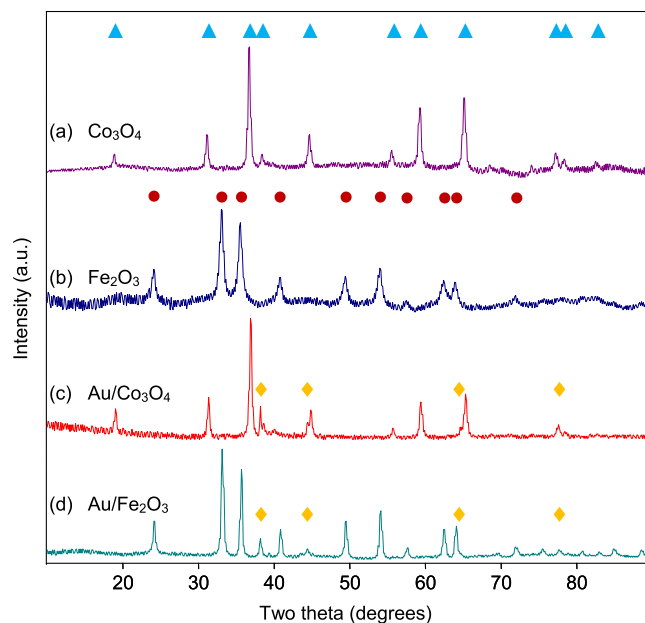
31.1 m^2 g^{-1} and 86.6 m^2 g^{-1} for cobalt oxide and iron oxide, respectively.

XRD patterns of cobalt oxide and iron oxide catalysts are shown in Fig. 3. The peak of XRD reflections are sharp and intense, suggesting well-crystallized phases of Co_3O_4 and Fe_2O_3 (hematite). The topography of iron oxide and cobalt oxide was investigated using Scanning Electron Microscopy (SEM). In the supplementary information (SI), the SEM images of Co_3O_4 and Fe_2O_3 are provided in Fig. S2 and Fig. S3 respectively, showing the surface morphologies of both samples. From these images we can see that the size distribution of cobalt oxide particles is narrower than iron oxide. Cobalt oxide has a nearly spherical shape and larger pore size compared to iron oxide.

The higher activity of Co_3O_4 catalyst compared to Fe_2O_3 catalyst was investigated using temperature-programmed desorption (TPD) of oxygen. Initially, both samples were heated in situ under vacuum up to 550 °C to remove any pre-adsorbed compounds. Oxygen (99.5%) was adsorbed at 400 °C followed by cooling to room

Fig. 2. Time on stream behaviour under dry and wet feed over Co_3O_4 (◯) and Fe_2O_3 (△) catalysts. Feed: 6000 ppm CH_4, 3 vol.% H_2O (for wet feed) balance air. GHSV = 100 000 h^{-1}, and bed temperature = 455 °C.

Fig. 3. X-ray diffraction patterns of (a) Co_3O_4, (b) Fe_2O_3, (c) Au/Co_3O_4 and (d) Au/Fe_2O_3 catalysts. Crystalline phase: ▲ = Co_3O_4, ● = Fe_2O_3, and ◆ = Au.
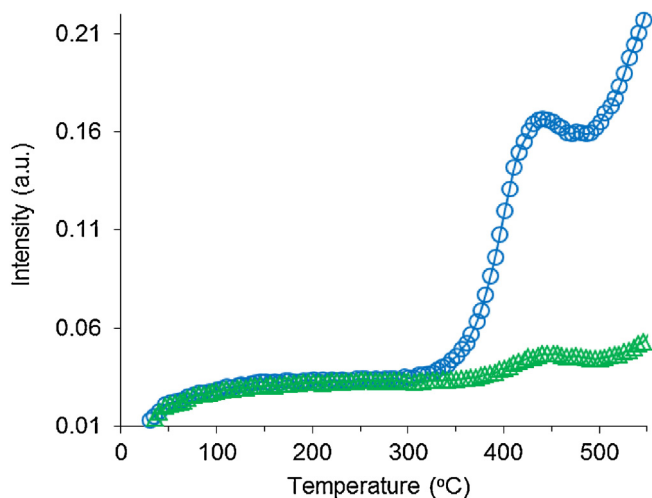
Fig. 4. TPD profile of O_2 desorption of Co_3O_4 ($\bigcirc$) and Fe_2O_3 ($\triangle$) catalysts at heating rate of $5\,^\circ C\,min^{-1}$. O_2 was adsorbed at $400\,^\circ C$.

temperature (RT). The TPD experiment was carried out with a temperature ramp of $5\,^\circ C\,min^{-1}$ heating from RT to $550\,^\circ C$. Fig. 4 shows the TPD profile of O_2 (m/z = 32) desorption over Co_3O_4 and Fe_2O_3 catalysts.

TPD spectra of Co_3O_4 suggests at temperature of $350\,^\circ C$ a significant concentration of oxygen is present on the surface, resulting in a maximum in the desorption rate of oxygen at $440\,^\circ C$. Meanwhile, over the surface of Fe_2O_3 the oxygen desorption starts at higher temperature ($400\,^\circ C$) and with a lower intensity. This is consistent with data from light-off curves plotted in Fig. 1 where between 300 and $400\,^\circ C$ observeable conversions were detected over both catalysts. The peaks at temperature in range of 350–$500\,^\circ C$ indicate that the oxygen adsorption capacity of Co_3O_4 catalyst is higher compared to Fe_2O_3 catalyst. The higher oxygen surface coverage of Co_3O_4 is suggested to be responsible for activity difference of the catalysts. As reported in the literature, it is inferred that, the re-oxidation of the reduced cobalt oxide sites is rate limiting [19,20].

The inhibiting effect of water was investigated using temperature-programmed-desorption analysis. Fig. 5 shows H_2O (m/z = 18) TPD spectra of (a) Co_3O_4 and (b) Fe_2O_3 catalysts where the water was adsorbed at $150\,^\circ C$ and TPD spectra recorded during desorption from RT to $650\,^\circ C$ with a heating rate of $5\,^\circ C\,min^{-1}$.

Prior to water adsorption, each sample was activated in situ at $400\,^\circ C$ for 1 h with a ramp of $5\,^\circ C\,min^{-1}$. Peak deconvolution of TPD spectra suggests four desorption states of water from both catalysts. The peak positions after curve fitting for all TPD samples are provided in Table S1 of SI. Three peaks were detected below $400\,^\circ C$. These peaks are related to desorption from weakly bond H_2O from the oxide surfaces. Above $400\,^\circ C$, a stronger bond of H_2O was detected from both samples. However, the intensity of water desorbed from Fe_2O_3 is higher than that of Co_3O_4 which suggests more water is bound to iron oxide than to Co_3O_4. Furthermore, the water desorption peak at ca $500\,^\circ C$ was found over Fe_2O_3 indicative of strongly bound water (hydroxyl) species. In light of this finding, the difference in catalytic activity can be explained by competition of the reactants with water or irreversible destruction of active sites. Rapid deactivation was observed over Fe_2O_3 catalyst (see Fig. 2) where the activity dropped from ca. 70% to 25% within 5 h methane oxidation using humid feed.

The surface composition and oxidation state of fresh and used samples were analyzed using XPS of Co_3O_4 and Fe_2O_3 catalysts. For this analysis, the fresh samples are the sample which has been activated (as mentioned in Section 2) and kept in a sealed container. The used samples are catalyst which have been used in time-on-stream (TOS) experiments, as plotted in Fig. 2. After the TOS run was terminated, the catalyst was transferred into the XPS sample chamber for analysis.

The experimental and fitted Co 2p spectra of fresh and used cobat oxide catalysts are presented in Fig. S4 of SI. As expected, the spectra of both samples are essentially identical, highlighting no change in oxidation state or surface composition following the time-on-stream experiments. This argument was cross-checked with fitted peak of O 1s spectra from both samples as shown in Fig. S5 of SI. At Co $2p_{3/2}$ the peak fitting suggests two cobalt species were detected at binding energies of 779.2 eV and 780.3 eV. Over the fresh sample, the peak at binding energy of 779.2 eV is identified as Co^{3+} and the peak at 780.3 eV is Co^{2+} [18,21]. It is noteworthy that no significant shift in binding energy was observed from the used sample. This XPS result is in line with the excellent stability of Co_3O_4 as observed during time-on-stream experiment (see Fig. 2).

Exploring an explanation for the rapid deactivation phenomena observed from iron oxide catalyst was investigated by collecting XPS of fresh and used Fe_2O_3 samples. The spectra at Fe 2p core
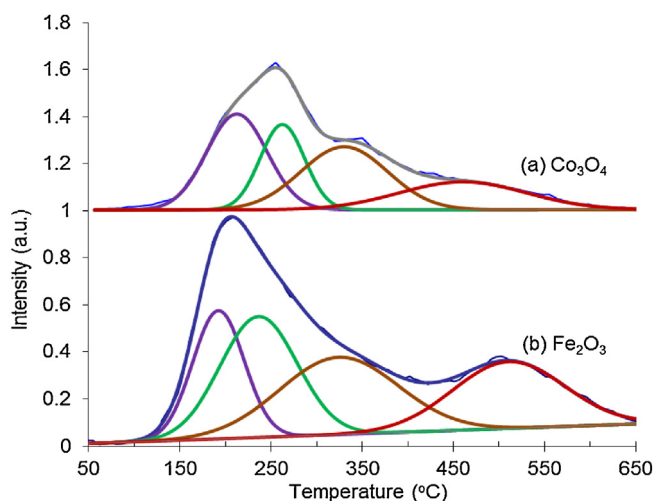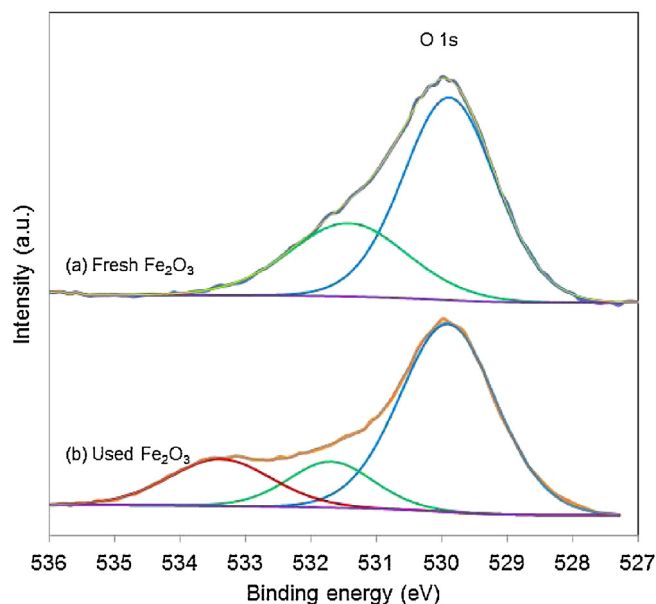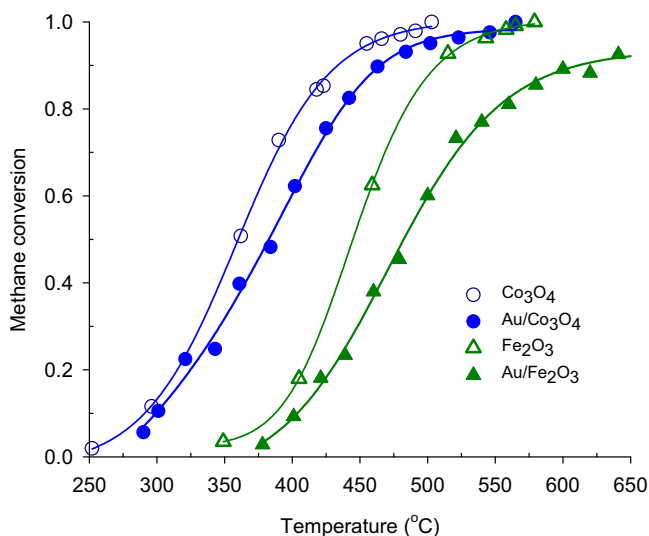

Fig. 5. TPD profile of H_2O desorption of (a) Co_3O_4 and (b) Fe_2O_3 catalysts at heating rate of $5\,^\circ C\,min^{-1}$, H_2O adsorption at $150\,^\circ C$. TPD spectra of Co_3O_4 were offset by 1 a.u. for clarity.

Fig. 6. XPS spectra of O 1s core level of (a) fresh Fe_2O_3 and (b) used Fe_2O_3.

Fig. 7. Methane conversion as a function of temperature over ($\bigcirc$) Co_3O_4, ($\bullet$) Au/Co_3O_4, ($\triangle$) Fe_2O_3 and ($\blacktriangle$) Au/Fe_2O_3 catalysts. Reaction condition: 6000 ppm CH_4 balance air at GHSV = 100 000 h^{-1}.

Fig. 8. Time on stream methane oxidation ($\bullet$) under dry and wet conditions over Au/Co_3O_4 catalyst at 455 °C; ($\square$) under dry conditions over Au/Fe_2O_3 catalyst at 530 °C; ($\blacktriangle$) under dry and wet conditions over Au/Fe_2O_3 catalyst at 530 °C; ($\triangle$) under dry and wet conditions over Fe_2O_3 catalyst at 455 °C. Reactant: 6000 ppm CH_4 balanced air, water vapour = 3 vol.%, GHSV = 100 000 h^{-1}.
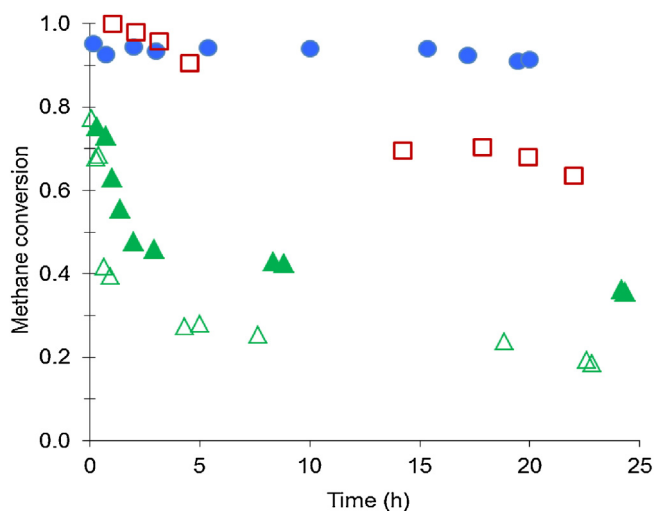
level for both samples are shown in Fig. S6 of SI. Comparison of these two spectra does not indicate any significant changes in oxidation state of Fe. Deconvolution of the peak under Fe $2p_{3/2}$ spectra results in two peaks at binding energies of 710 ± 0.2 eV and 711.3 ± 0.1 eV. As suggested in the literature, these peaks are attributed to Fe^{3+} species [22,23] which is typically the oxidation state of Fe_2O_3 (haematite). This argument is consistant with the XRD patterns of both samples, the result suggesting the dominance of haematite phase in these samples.

The fitted peak and the experimental spectra of O 1s core-level of fresh and used Fe_2O_3 are plotted in Fig. 6. The spectra of fresh sample (Fig. 6a) suggests two peaks at binding energies of 529.9 eV and 531.4 eV while deconvolution of the used Fe_2O_3 spectra (Fig. 6b) results in three peaks at binding energies of 529.9 eV, 531.7 eV and 533.4 eV. The presence of a peak at binding energy of 533.4 eV over the used sample is most-likely related to the formation of hydroxyl species on the surface of Fe_2O_3, which is consistent with data reported in the literature [24,25].

3.3. Dependency of activity and stability of Au supported on Co_3O_4 and Fe_2O_3

The catalytic activity and stability of cobalt oxide and iron oxide were further evaluated following the loading of Au particles on these supports using a co-precipitation method, as outlined in the experimental section. Fig. 7 shows the temperature dependency of methane conversion over Au/Co_3O_4 and Au/Fe_2O_3 catalysts compared with the data plotted for single oxide catalysts in Fig. 1.

The temperature of 10% conversion varies significantly, with the Co_3O_4 exhibiting the lowest light-off temperature. This figure suggests that the nano-sized cobalt oxide is the most active catalyst, followed by Au/Co_3O_4, Fe_2O_3 and Au/Fe_2O_3 catalysts. The temperatures at 10% methane conversion (T_{10}) for Co_3O_4 and Au/Co_3O_4 are similar (suggesting similar intrinsic rates). The T_{90} of Co_3O_4 is about 50 °C lower than the temperature of 90% methane conversion over Au/Co_3O_4. Comparison of Fe_2O_3 and Au/Fe_2O_3 light-off curves also suggests that the support material is more active than the supported gold catalyst. At 500 °C methane oxidation over Fe_2O_3 catalyst achieves 90% conversion level while Au/Fe_2O_3 catalyst can only convert 60% of CH_4 into CO_2. Surprisingly, the presence of gold on cobalt oxide or iron oxide does not enhance the activity of the catalyst, if it has any influence that

effect appears to be detrimental in terms of catalytic activity. This behaviour suggests potential poisoning of transition metal sites by gold, the details of which are currently under investigation.

The activity of the catalysts at different space velocities was investigated over Au/Co_3O_4 and Au/Fe_2O_3 catalysts. In Fig. S7 and Fig. S8 of the supplementary information (SI), we plot the light-off curves for methane oxidation over Au/Co_3O_4 and Au/Fe_2O_3 catalysts. A drop in T_{90} of 30 °C in activity was observed from Au/Co_3O_4 catalyst when varying the GHSV from 27 000 h^{-1} to 100 000 h^{-1}, while over Au/Fe_2O_3 catalyst the temperature at 90% conversion (T_{90}) was shifted up about 100 °C upon increasing the space velocity from 35 000 h^{-1} to 100 000 h^{-1}. This result is consistent with the data reported by Choudhary et al. where the activity of Au/Fe_2O_3 catalyst was significantly affected by changing GHSVs [11].

The stability of gold supported on cobalt oxide and gold supported on iron oxide catalysts were evaluated under similar condition as mentioned above. Initially, the experiment was started by feeding the reactor with dry feed for 45 min, and then switched to wet feed (dry and wet conditions). Fig. 8 shows the time-on-stream evolution of methane combustion over these catalysts for 24 h. For comparison, TOS data of Fe_2O_3 (dry wet conditions) and Au/Fe_2O_3 tested under dry feed conditions are plotted also in this figure. The activity of Au/Co_3O_4 catalyst is fairly constant before and after water vapour was introduced into the feed, similar to what was observed from Co_3O_4 catalyst (see Fig. 2). In contrast, over Au/Fe_2O_3 catalyst, the presence of water in the feed leads to significant deactivation. However, the deactivation rate of Au/Fe_2O_3 catalyst is lower compared to deactivation rate of Fe_2O_3 catalyst. This observation is likely due to a higher reaction temperature for TOS experiment of Au/Fe_2O_3 catalyst. As suggested by TPD spectra (see below), at 530 °C less water remains on the surface. In addition, the dry feed TOS experiment of Au/Fe_2O_3 catalyst at 530 °C indicates that removing water from the feed decreases the deactivation rate. This is consistent with our findings from TPD and XPS analyses from which we conclude that the hydroxyl species are strongly bonded on the surface.

The surface area of the samples calculated from N_2-physisorption data using BET equation are provided in Table 1. Compared with co-precipitated gold on iron oxide catalyst, the pure iron oxide exhibits higher surface area due to modified preparation method. Meanwhile, pure cobalt oxide and supported gold on
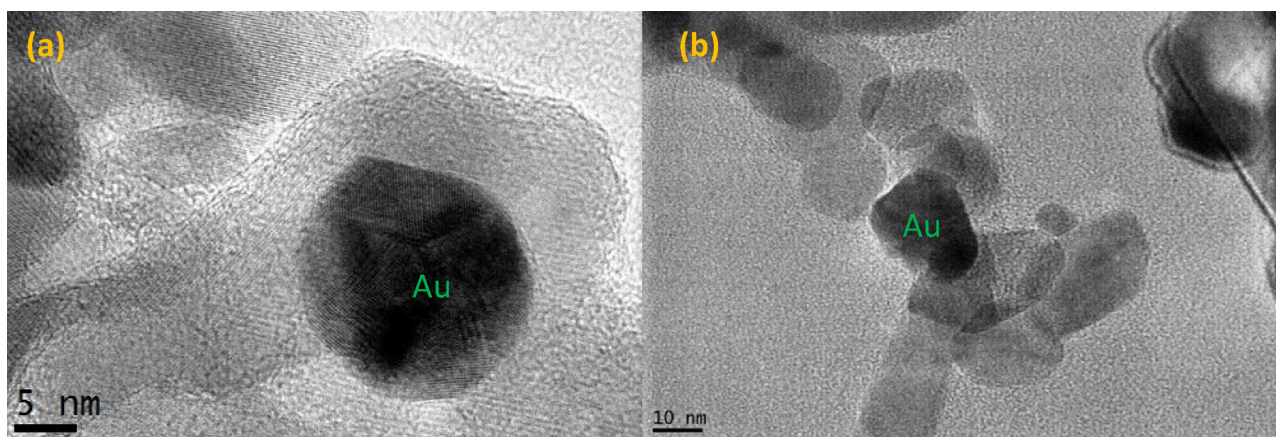
Fig. 9. HR-TEM images of (a) Au/Fe_2O_3 and (b) Au/Co_3O_4 catalysts.

Table 1
Surface area and Au particle size.

Sample	BET surface area ($m^2\,g^{-1}$)	Average Au particle size measured by TEM (nm)
1.7 wt.% Au/Fe_2O_3	55.5	15
2.2 wt.% Au/Co_3O_4	32.9	18
Co_3O_4	31.1	–
Fe_2O_3	86.6	–

cobalt oxide catalyst have similar specific surface areas. The ICP-OES results confirm the presence of 1.7 wt% and 2.2 wt% of gold on iron oxide and cobalt oxide, respectively.

XRD patterns of gold supported on cobalt oxide and iron oxide catalysts are shown in Fig. 3c and d. The XRD reflections are sharp and intense suggesting well-crystallized phases of Au, Fe_2O_3 and Co_3O_4. The line broadening of the highest intensity of the gold reflection peak suggests that the crystallite size of both samples is similar. This is supported by particle size measurement using TEM analysis where the average gold particle size of Au/Co_3O_4 and Au/Fe_2O_3 are 18 nm and 15 nm, respectively. It was also observed that the line broadening at half the maximum intensity (FWHM) of Co_3O_4 reflection at $36.8°$ 2θ decreased slightly following gold deposition. Our calculation suggests that the cobalt oxide particle size increased about 3 nm upon loading gold on the oxide. This is supported by the surface area calculation results in Table 1 where no significant increase was observed after gold deposition on Co_3O_4. Please note that the differences in FWHM of Fe_2O_3 reflections observed in our samples are due to different precursor used.

The distribution of gold nano particles on Fe_2O_3 (Fig. S9 of SI) and Co_3O_4 (Fig. S10 of SI) was successfully recorded by using backscattered electron (BE) detector. From these images, well dispersed bright-colour-dots are evident, which are identified as gold particles and later confirmed by EDS analysis. High resolution micrographs of gold catalysts captured by TEM are presented in Fig. 9. The gold particle deposited on Fe_2O_3 is shown in Fig. 9a and the gold supported on Co_3O_4 is in Fig. 9b. In general, the Au particle size observed is in the range of 8–30 nm. TEM image and particle distribution are provided in Fig. S11 of SI and suggests an average particle size of 18 nm, significantly higher than the particle size suggested for optimal activity of supported Au catalysts [26].

The influence of gold particle size in methane oxidation was reported by Blick et al. [27], who found that gold particles with diameter of 5–10 nm supported on MgO were active for converting methane into CO and CO_2. The same effect was observed also over Au/Al_2O_3 catalysts prepared by impregnation and deposition-precipitation methods where the smallest particle sizes (3–5 nm) were found to be the most active [28]. An enhanced catalytic
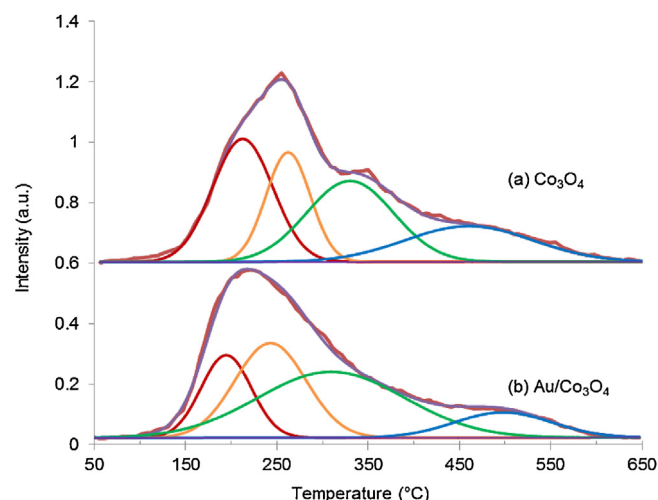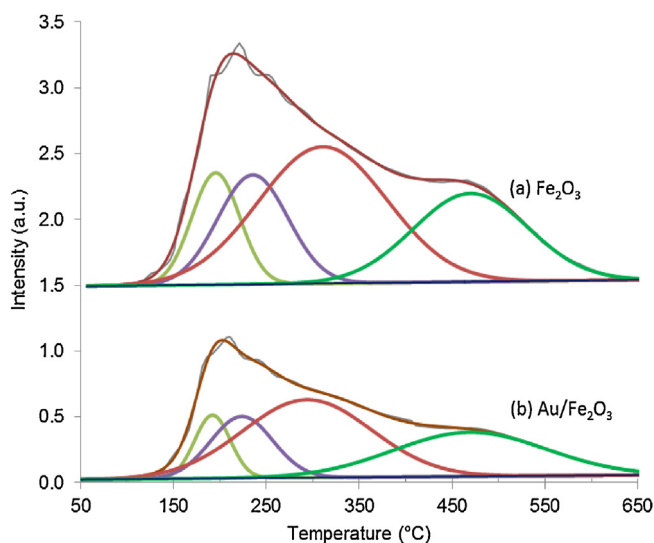

Fig. 10. TPD profile of H_2O desorption of (a) Co_3O_4 and (b) Au/Co_3O_4 catalysts at heating rate of $5\,°C\,min^{-1}$, H_2O adsorption at $150\,°C$. Plot (a) was offset by 0.6 a.u. to improve clarity.

activity of the nano-sized gold (8–9 nm) was demonstrated recently upon loading 10 wt% of Au on Co_3O_4 [21]. However, in our samples, the gold loading was below 3 wt% and the average gold particle size is 18 nm for Au/Co_3O_4 catalysts (based on TEM analysis). It was expected that loading the gold to the metal oxide catalyst surface would produce an increase in catalytic activity, however the gold particle in the samples tested does not enhance methane conversion (see Fig. 7).

The inhibiting effect of water was investigated for Au supported on Co_3O_4 and Fe_2O_3 catalysts. Fig. 10 shows H_2O-TPD spectra of Au/Co_3O_4 in comparison with spectra of Co_3O_4 catalysts where the water was adsorbed under similar condition as described above. Peak fitting of TPD spectra suggests four desorption states of water from Au/Co_3O_4 catalysts at temperatures of $195\,°C$, $243\,°C$, $309\,°C$ and $498\,°C$. These peak positions have shifted slightly in comparison to the position of the peaks found for desorption from Co_3O_4 which is related to the loading Au on Co_3O_4.

TPD spectra of water desorbed from Fe_2O_3 catalyst were compared with the spectra obtained from Au/Fe_2O_3 catalysts, in order to explore the interaction between the hydroxyl groups on the catalyst, the gold and support. Both spectra are shown in Fig. 11. Gaussian peak fitting of Au/Fe_2O_3 TPD spectra suggests four adsorption states of water resulting in desorption peaks at temperatures of $192\,°C$, $224\,°C$, $294\,°C$ and $469\,°C$. These peaks are similar to those found for water desorption from Fe_2O_3. It is interesting to
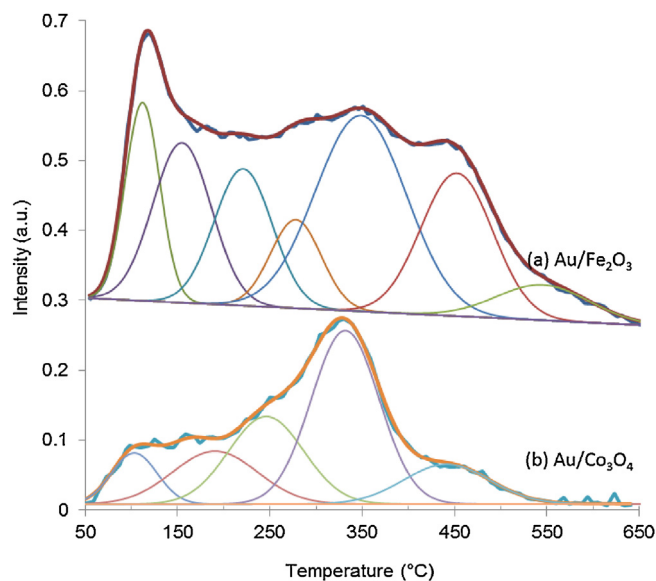
Fig. 11. TPD profile of H_2O desorption of (a) Fe_2O_3 and (b) Au/Fe_2O_3 catalysts at heating rate of $5\,°C\,min^{-1}$, H_2O adsorption at $150\,°C$. Plot (a) was offset by 1.5 a.u. for clarity.

Fig. 12. TPD profile of H_2O desorption over (a) used Au/Fe_2O_3 and (b) used Au/Co_3O_4 catalysts. H_2O was adsorbed during TOS experiment as plotted in Fig. 8. Plot (a) was offset by a straight line for better visualization.

see that upon loading gold on the iron oxide, no new adsorption sites (desorption peaks) were detected. Evidence for interaction between water and gold was essentially absent from these spectra. This suggests that most of water was adsorbed on Fe_2O_3. This is consistent with our XPS result below, where hydroxyl species were detected on the sample that was used for time-on-stream experiments under humid condition.

The water and catalyst interaction during catalytic combustion of methane was investigated using TPD analysis of used gold catalysts (TOS experiments as plotted in Fig. 8). After the TOS experiment was terminated, the catalyst was purged with helium while cooling in the furnace to room temperature. The sample was immediately transferred into a TPD tube. Desorption of H_2O was then started from $30\,°C$ until $650\,°C$ at heating rate of $5\,°C\,min^{-1}$. Fig. 12 shows the TPD spectra of water which was adsorbed on the surface of Au/Fe_2O_3 and Au/Co_3O_4 catalysts during TOS experiments.

As shown in Fig. 12, TPD spectra of Au/Fe_2O_3 catalyst can be fitted based on seven distinct sites for H_2O adsorption. The main water desorption sites were observed at $120\,°C$, $350\,°C$ and $450\,°C$. The peak at $120\,°C$ is the most intense peak, which can be interpreted as the weakest bond of hydroxyl compounds adsorbed on Au/Fe_2O_3 catalyst, whereas the peaks at higher temperatures are mostly related to hydroxyl compounds adsorbed during time-on-stream experiment under wet feed as described in Fig. 8. As expected, TPD analysis of used Au/Co_3O_4 catalyst results in a lower net H_2O coverage and in turn less prominent desorption peaks compared to that of Au/Fe_2O_3 catalyst. Curve fitting suggests that there are five peaks at temperatures of $103\,°C$, $161\,°C$, $246\,°C$, $332\,°C$ and $441\,°C$, respectively. The most intense peak is at $332\,°C$ while the smallest peak is at $441\,°C$. It is suggested that at $441\,°C$, very little H_2O is adsorbed on the surface of Au/Co_3O_4 catalyst when compared to Au supported on Fe_2O_3. As a result, we speculate that the presence of water during time-on-stream experiment over Au/Co_3O_4 (see
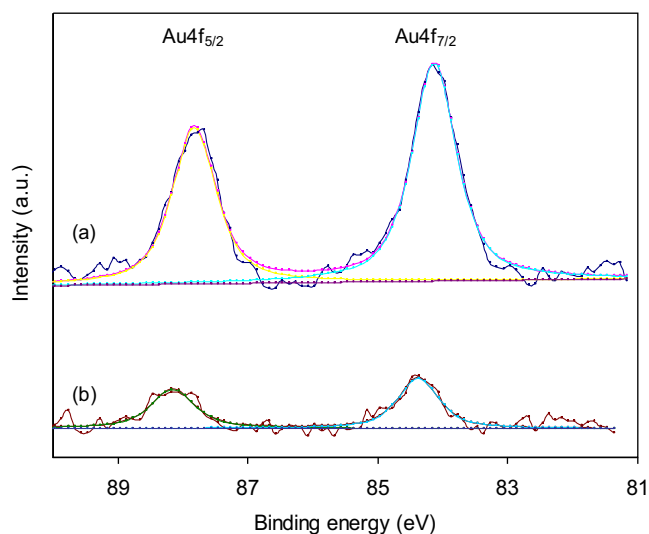
Fig. 13. XPS spectra of Au 4f core level of (a) Au/Fe_2O_3 and (b) Au/Co_3O_4 catalysts.

Fig. 8) has, similar to the Co_3O_4 support, little effect on methane combustion.

The oxidation state and surface composition of 1.7 wt% Au/Fe_2O_3 and 2.2 wt% Au/Co_3O_4 catalysts were analyzed with XPS. Both samples were calcined ex situ in air at $400\,°C$ for 4 h before loading to the XPS sample holder. The spectra of Au 4f core level region are plotted in Fig. 13 and the surface composition is provided in Table 2. Deconvolution of the peak under the curve at Au $4f_{7/2}$ core-level was performed using Gaussian–Lorentzian (30:70) peak shapes. There is a single element detected at binding energies (BE's) of 84.1 eV and 84.4 eV for Au/Fe_2O_3 and Au/Co_3O_4, respectively

Table 2
XPS peak position and surface composition.

Sample	Au 4f peak position (eV)		Surface composition (%)				
	Au4f$_{7/2}$	Au4f$_{5/2}$	Au	O	Fe	Co	C
a.	1.7 Au/Fe$_2$O$_3$	84.1	87.8	0.14	61.6	32.6	–	4.21
b.	2.2 Au/Co$_3$O$_4$	84.4	88.2	0.05	58.9	–	35.6	2.94

(FWHM = 0.84–0.89 eV). From each sample, the single peak is identified as Au^0 which is consistent with the binding energies reported in the literature [21,29]. It is interesting to note that the Au peak on Au/Co_3O_4 is small, (see Table 2), indicating only a low surface concentration of Au. This result is consistent with our finding from TPD analysis. Comparison of Co_3O_4 and Au/Co_3O_4 TPD spectra (Fig. 10) suggests that the H_2O desorption temperatures and in turn adsorption energies of both samples are similar.

4. Conclusions

The activity and hydrothermal stability of Co_3O_4, Fe_2O_3, Au/Co_3O_4 and Au/Fe_2O_3 catalysts were evaluated for catalytic combustion of lean air-methane mixtures. Excellent stability was observed over nano-particle Co_3O_4 and Au/Co_3O_4 during time-on-stream experiments. No changes in oxidation/chemical states were observed from Co_3O_4 catalyst, before and after TOS experiments. The presence of strongly bonded adsorption of hydroxyl species on the surface of all catalysts studied, as observed by TPD and XPS analyses, highlights the role of water as being responsible for the rapid deactivation over Fe_2O_3 and Au/Fe_2O_3 catalysts. Nevertheless, co-precipitating gold with cobalt oxide or iron oxide does not enhance the activity of the catalyst.

Acknowledgements

Appendix A. Supplementary data

Supplementary data associated with this article can be found, in the online version, at http://dx.doi.org/10.1016/j.cattod.2014.11.031.

References

[1] S. Solomon, D. Qin, M. Manning, Z. Chen, M. Marquis, K.B. Averyt, M. Tignor, H.L. Miller, Fourth Assessment Report: Climate Change 2007. The Physical Science Basis, Contribution of Working Group I to the Fourth Assessment Report of the Intergovernmental Panel on Climate Change 2007, Cambridge University Press, Cambridge, United Kingdom and New York, NY, USA, 2007.

[2] J.K. Stolaroff, S. Bhattacharyya, C.A. Smith, W.L. Bourcier, P.J. Cameron-Smith, R.D. Aines, Environ. Sci. Technol. 46 (2012) 6455–6469.

[3] P. Gelin, M. Primet, Appl. Catal. B 39 (2002) 1–37.

[4] A. Setiawan, J. Friggieri, E.M. Kennedy, B.Z. Dlugogorski, M. Stockenhuber, Catal. Sci. Technol. 4 (6) (2014) 1793–1802.

[5] G.C. Bond, Catal. Today 72 (2002) 5–9.

[6] M. Haruta, T. Kobayashi, H. Sano, N. Yamada, Chem. Lett. (1987) 405–408.

[7] R.D. Waters, J.J. Weimer, J.E. Smith, Catal. Lett. 30 (1995) 181–188.

[8] R.J.H. Grisel, B.E. Nieuwenhuys, Catal. Today 64 (2001) 69–81.

[9] S. Miao, Y. Deng, Appl. Catal. B 31 (2001) L1–L2.

[10] B.E. Solsona, T. Garcia, C. Jones, S.H. Taylor, A.F. Carley, G.J. Hutchings, Appl. Catal. A 312 (2006) 67–76.

[11] V.R. Choudhary, V.P. Patil, P. Jana, B.S. Uphade, Appl. Catal. A 350 (2008) 186–190.

[12] T.V. Choudhary, S. Banerjee, V.R. Choudhary, Appl. Catal. A 234 (2002) 1–23.

[13] J.R. Paredes, E. Diaz, F.V. Diez, S. Ordonez, Energy Fuels 23 (2009) 86–93.

[14] L. Hu, Q. Peng, Y. Li, J. Am. Chem. Soc. 130 (2008) 16136–16137.

[15] Z. Fei, S. He, L. Li, W. Ji, C.-T. Au, Chem. Commun. (Cambridge, UK) 48 (2012) 853–855.

[16] Y. Liu, H. Tuysuz, C.-J. Jia, M. Schwickardi, R. Rinaldi, A.-H. Lu, W. Schmidt, F. Schuth, Chem. Commun. (Cambridge, UK) 46 (2010) 1238–1240.

[17] A. Setiawan, E.M. Kennedy, B.Z. Dlugogorski, A.A. Adesina, O. Tkachenko, M. Stockenhuber, Energy Technol. (Weinheim Ger.) 2 (2014).

[18] Y. Liu, H. Dai, J. Deng, S. Xie, H. Yang, W. Tan, W. Han, Y. Jiang, G. Guo, J. Catal. 309 (2014) 408–418.

[19] N. Bahlawane, Appl. Catal. B: Environ. 67 (2006) 168–176.

[20] L.F. Liotta, H. Wu, G. Pantaleo, A.M. Venezia, Catal. Sci. Technol. 3 (2013) 3085–3102.

[21] L.F. Liotta, G. DiCarlo, A. Longo, G. Pantaleo, A.M. Venezia, Catal. Today 139 (2008) 174–179.

[22] Y. Zhang, T. Ma, J. Zhao, J. Catal. 313 (2014) 92–103.

[23] A.P. Grosvenor, B.A. Kobe, M.C. Biesinger, N.S. McIntyre, Surf. Interface Anal. 36 (2004) 1564–1574.

[24] S.D. Senanayake, D. Stacchiola, P. Liu, C.B. Mullins, J. Hrbek, J.A. Rodriguez, J. Phys. Chem. C 113 (2009) 19536–19544.

[25] A.V. Naumkin, A. Kraut-Vass, S.W. Gaarenstroom, C.J. Powell, NIST Standard Reference Database 20, Version 4.1, 2012, http://srdata.nist.gov/xps/

[26] M. Haruta, Catal. Today 36 (1997) 153–166.

[27] K. Blick, T.D. Mitrelias, J.S.J. Hargreaves, G.J. Hutchings, R.W. Joyner, C.J. Kiely, F.E. Wagner, Catal. Lett. 50 (1998) 211–218.

[28] R.J.H. Grisel, P.J. Kooyman, B.E. Nieuwenhuys, J. Catal. 191 (2000) 430–437.

[29] B. Solsona, M. Pérez-Cabero, I. Vázquez, A. Dejoz, T. García, J. Álvarez-Rodríguez, J. El-Haskouri, D. Beltrán, P. Amorós, Chem. Eng. J. 187 (2012) 391–400.